Journal of Hazardous Materials 492 (2025) 138261

Contents lists available at ScienceDirect

Journal of Hazardous Materials

journal homepage: www.elsevier.com/locate/jhazmat

Enhanced sulfamethoxazole removal in water and wastewater by ferrate (VI)/perborate system via borate buffering

Zihe Chen [a], Cong Li [a,*], Jingzhen Su [a], Zhenming He [a], Jiani Xu [a], Yulin Bian [a], Hyunook Kim [b], Xiaohong Guan [c]

[a] School of Environment and Architecture, University of Shanghai for Science and Technology, Shanghai 200093, China
[b] University of Seoul, Dept. of Environmental Engineering, 163 Seoulsiripdae-ro, Dongdaemun-gu, Seoul 02504, South Korea
[c] Shanghai Engineering Research Center of Biotransformation of Organic Solid Waste, Institute of Eco-Chongming, School of Ecological and Environmental Sciences, East China Normal University, Shanghai 200241, China

HIGHLIGHTS

- The Fe(VI)/perborate system is proposed for the first time.
- The borate produced by sodium perborate acts as a buffer for Fe(VI).
- The Fenton reaction between H_2O_2, Fe (II) and Fe(III) produced in the Fe(VI)/perborate system.
- Fe(VI)/perborate system maintained efficient degradation of SMX in WWTP secondary effluent.
- Fe(VI)/perborate system has high degradation ability for different antibiotics.

GRAPHICAL ABSTRACT

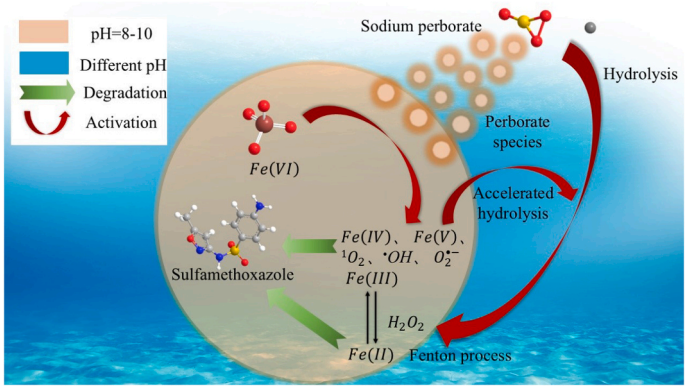

ARTICLE INFO

Keywords:
Ferrate
Perborate
Wastewater treatment
Buffering capacity
Sulfamethoxazole

ABSTRACT

Ferrate(VI) is prone to self-decomposition in water, leading to the loss of active substances Fe(V) and Fe(IV). Therefore, the use of Fe(VI) alone has limited practical applicability in municipal wastewater and industrial wastewater treatment scenarios due to its insufficient pollutant removal efficiency. This study discussed the removal efficiency of the Fe(VI)/perborate system for sulfamethoxazole and other 6 drugs in pure water within 5 minutes, and the removal efficiency of the Fe(VI)/perborate system for sulfamethoxazole in effluent and secondary effluent in a wastewater treatment plant (WWTP) within 5 minutes. Results show that the sulfamethoxazole removal efficiency reached 88.63 % in the influent of Lijiang B WWTP and 79 % in the secondary effluent of Wuhan WWTP. The removal efficiency of sulfamethoxazole in pure water reached 25.8 % in 5 minutes. This finding is explained by the buffering with the borate produced by the hydrolysis of Fe(VI)/perborate, which maintains the pH around 9 and, in turn, inhibits the reduction of active species. Moreover, H_2O_2, $^1O_2$, and $O_2^{\bullet-}$ radicals generated by Fe(VI)/perborate accelerate the activation of Fe(VI), and the Fe^{2+} produced in the

* Corresponding author.
E-mail address: licong@usst.edu.cn (C. Li).

https://doi.org/10.1016/j.jhazmat.2025.138261
Received 30 December 2024; Received in revised form 10 April 2025; Accepted 10 April 2025
Available online 11 April 2025

system participates in Fenton reactions with H_2O_2. This study offers a novel approach for using ferrate in practical water treatment.

1. Introduction

In the post-pandemic era of COVID-19, sulfamethoxazole, a sulfonamide antibiotic, has been widely utilized in combating the pandemic [4]. sulfamethoxazole is discharged into aquatic environments through pharmaceutical wastewater, hospital effluents, and domestic sewage, leading to its widespread detection in various natural water bodies [35]. Conventional wastewater treatment processes in sewage treatment plants achieve only about 20 % removal efficiency for sulfonamide antibiotics [36]. Due to its chemically stable structure and resistance to photodegradation, sulfamethoxazole persists in aqueous matrices for extended periods [9]. Therefore, an effective water treatment technology is required to efficiently remove sulfamethoxazole from contaminated water.

In recent years, research on ferrate has focused on the combined use of Fe(VI) with peracetic acid, persulfates, percarbonate, and other peroxides to degrade emerging contaminants [28]. However, persulfates are not widely applicable in practical water treatment due to their high cost [45]. Peracetic acid, when its concentration exceeds 40 %, poses an explosion risk, making it difficult to store and transport. Furthermore, contact with peracetic acid can cause damage to human skin and mucous membranes, posing safety concerns [21]. Previous studies have shown that systems coupling Fe(VI) with other oxidants are often susceptible to interference from external factors. For instance, in the Fe(VI)/PAA system, the pH of the reaction mixture significantly varies with different ferrate concentrations [23]. The coupling of Fe(VI) with H_2O_2 in water treatment applications faces practical challenges, such as the inconvenience of H_2O_2 transportation. Sodium perborate is a novel solid powder oxidant widely used in products for cleaning and laundry, such as bleach [29]. Sodium perborate is characterized by its high oxygen content, low solubility in water, and strong oxidative properties. It can be stored at room temperature, making it convenient for transportation and handling [55]. Sodium perborate is a mild pH modifier that enhances the efficiency of iron ion utilization in aqueous solutions [54]. Upon hydrolysis, sodium perborate generates hydrogen peroxide (H_2O_2), which reacts with the Fe^{2+} ions produced by the activation of ferrate, facilitating the Fenton reaction and increase the removal rate of pollutants [40]. When dissolved in water, sodium perborate continuously releases hydrogen peroxide, contributing to its bleaching effect. Additionally, sodium perborate undergoes hydrolysis to form sodium metaborate ($NaBO_2$), which further hydrolyzes to produce H_3BO_3 and $B(OH)_4^-$ (pKa = 9.2), maintaining a pH around 9. This pH buffering capacity helps the system resist external pH fluctuations [17]. Currently, no studies have reported on the coupled oxidation system of sodium perborate and Fe(VI). Previous research on Fe(VI)-based water treatment typically involved dissolving Fe(VI) in a borate solution before mixing it with the pollutant-containing aqueous solution [46]. This approach aims to maintain an alkaline environment to preserve Fe(VI) activity, suppress its self-decomposition, and ensure its high oxidation efficiency [53]. Therefore, these characteristics make sodium perborate a promising candidate for water treatment applications, and thus, the Fe(VI)/perborate system has been investigated for its potential in water purification.

Ferrate is commonly utilized in water treatment processes [6]. With an oxidation potential of 2.20 eV, ferrate is capable of efficiently degrading persistent organic pollutants, heavy metals, and micropollutants, while also being environmentally friendly [6,26]. The final products of ferrate are Fe(III) and Fe(II). In most studies involving ferrate, sodium borate is commonly used to prepare ferrate stock solutions, as ferrate tends to decompose rapidly in water, leading to the loss of active species like Fe(V) and Fe(IV) [10]. However, in borate solution, the self-decomposition rate of ferrate is significantly slowed, thus preserving the concentration of active species, Fe(V) and Fe(IV) [43]. Based on these findings, this study hypothesizes that when ferrate is combined with sodium perborate, the H_2O_2 generated by the hydrolysis of sodium perborate will not only activate Fe(VI) to convert to Fe(V) and Fe(IV), but also generate singlet oxygen ($^1O_2$) and superoxide anion ($O_2^{\bullet-}$) [55]. Moreover, Fe(VI) and $H_3BO_3/B(OH)_4^-$ will further produce HOOBO/-HOOB$(OH)_3$, continuously generating reactive oxygen species such as $O_2^{\bullet-}$, $^1O_2$, $^{\bullet}OH$. Simultaneously, the borate solution formed will help maintain the pH of the system around 9, minimizing the loss of active species and enabling sustained, efficient degradation of sulfamethoxazole.

The objectives of this study were to: (1) examine the removal efficiency of the Fe(VI)/perborate system on sulfamethoxazole under various influencing factors, (2) investigate its effects on the degradation of different pollutants, (3) analyze the types of reactive species present in the system and the mechanisms behind their formation, (4) analyze the effectiveness of the Fe(VI)/perborate system in degrading sulfamethoxazole in real wastewater treatment processes, (5) conduct DFT simulations and degradation pathway analysis for sulfamethoxazole, and (6) assess the toxicity changes during the degradation process.

2. Materials and methods

2.1. Materials

The chemical reagents used in this experiment are detailed in Text S1. Tables S1 and S2 shown the WWTP influent and secondary effluent water quality indicators in Lijiang (A, B, C) and Dali, Qujing, Baoshan, Yunan province, and Wuhan, Hubei province.

In this experiment, Fe(VI) was prepared using a wet method. First, potassium permanganate, concentrated hydrochloric acid, potassium hydroxide, and ferric nitrate nonahydrate were used to synthesize the Fe (VI) sample. The obtained sample was washed with organic reagents such as n-pentane, methanol, and ether to obtain high-purity Fe(VI) (≥95 %), based on previous methods for Fe(VI) synthesis, an optimized approach was developed using hypochlorite-driven oxidative conversion of $Fe(NO_3)_3$ [13]. Finally, the solid K_2FeO_4 was multilayered with glass filter paper and stored in a sealed condition under low-temperature drying.

2.2. Experimental procedures

The experiment utilized the equal-volume reaction method [7]. 0.1 mol/L NaOH and HCl solutions were used to regulate the reaction mixture's initial pH. The experiment was carried out in pure water. In the experimental section on SMX degradation efficiency in influent and effluent from a wastewater treatment plant, 5 mL of 0.2 mM SMX was added to 45 mL of influent and effluent, respectively, resulting in a final SMX concentration of 0.02 mM. This setup was used to investigate the degradation behavior of sulfamethoxazole in real wastewater. The Fe (VI)/perborate system took place in a 100 mL beaker, with a reaction volume of 50 mL. The Fe(VI) and sodium perborate were added stepwise in concentration gradients [32]. Fe(VI) and sodium perborate were directly added to the reaction mixture at 0 minutes, with solid Fe(VI) and sodium perborate being simultaneously introduced into the solution to initiate the SMX degradation process. Both systems were stirred at 300 rpm utilizing a magnetic stirrer to guarantee sufficient interaction between the contaminants and oxidants. At the beginning of the experiment, At specified intervals, 1 mL samples were taken. These samples were then added to centrifuge tubes containing 300 μL of

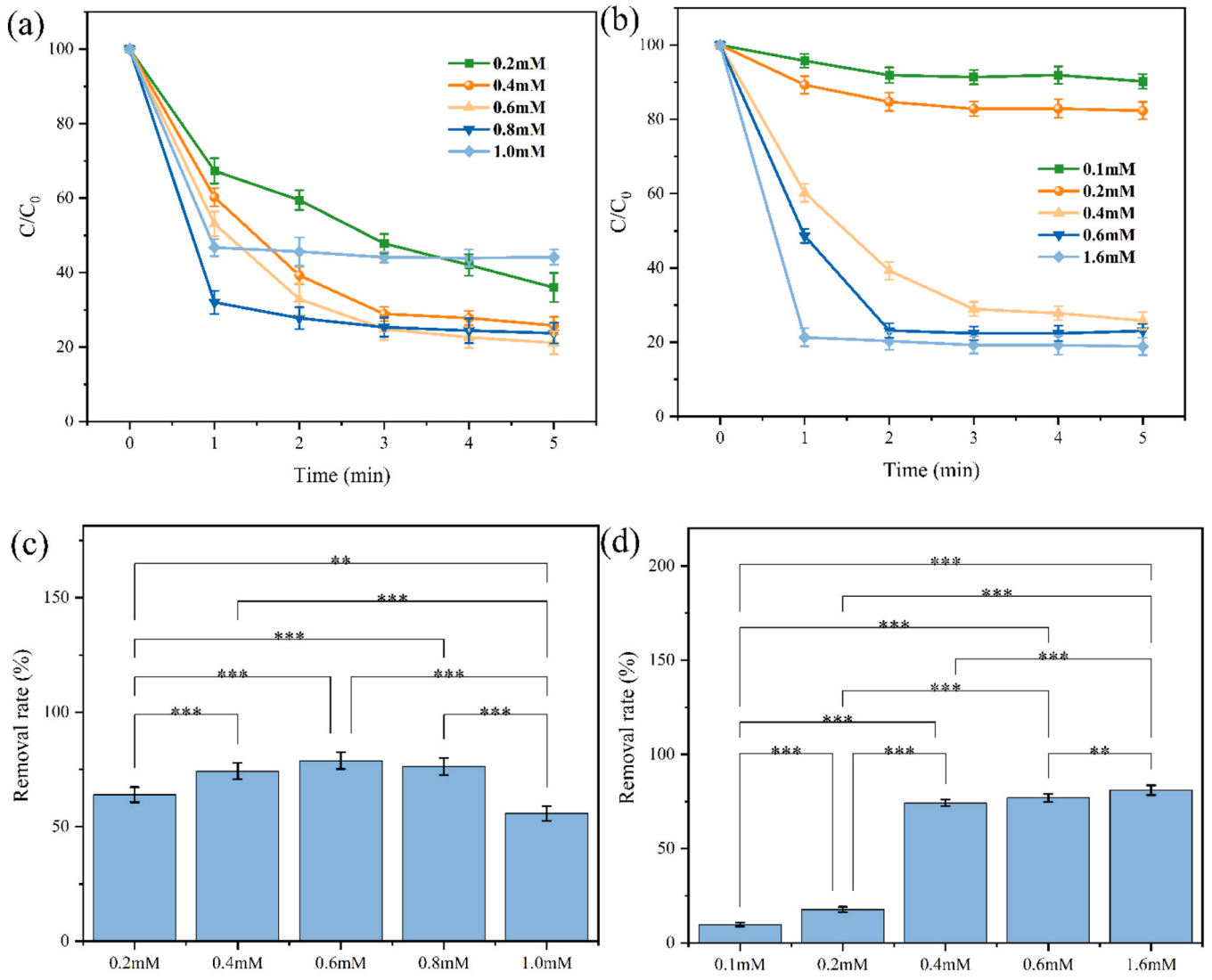

Fig. 1. Removal efficiency of sulfamethoxazole at (a) different sodium perborate concentrations and (b) different Fe (VI) concentrations, (c) Effects of sodium perborate with different concentrations on SMX removal rate at 5 min. (d) Effects of Fe(VI) with different concentrations on SMX removal rate at 5 min. Conditions: [sulfamethoxazole] = 0.02 mM, [Fe(VI)] = 0.1–1.6 mM, [$NaBO_3$] = 0.2–1.0 mM, pH_0 = 9.2, T = 25°C. "*" represents significant differences in the one-way ANOVA, where "*" means $p \leq 0.05$, "**" means $p \leq 0.01$, and "***" means $p \leq 0.001$.

1 mol/L sodium thiosulfate quenching agent to stop the reaction. After quenching, the samples were filtered through a 0.25 μm hydrophilic polyethersulfone syringe filter (Shanghai ANPEL, China) and transferred to sample vials. Finally, the concentration of sulfamethoxazole was analyzed using High-Performance Liquid Chromatography (HPLC). Each experimental group was repeated three times to minimize errors. The details of the quenching agents used in the experiments are provided in Table S3.

The removal efficiency of drugs was evaluated based on removal efficiency and rate constants. The removal of drugs follows a pseudo-first-order kinetic model:

$$\ln\frac{C_t}{C_0} = -\text{kobst} \quad (1)$$

The concentrations of drugs at time t and time 0 are denoted as C_t and C_0, respectively, while k_{obs} represents the removal rate constant.

2.3. Analytical methods

The concentrations of sulfamethoxazole, ciprofloxacin, carbamazepine, amoxicillin, ibuprofen, tetracycline, and metronidazole before and after the reaction were quantified using HPLC (Shimadzu HPLC-2030, Japan). The system was set up with a UV detector, and Chromatographic separation was performed with a 150 mm × 4.6 mm C18 column. Detailed analytical procedures are outlined in Table S4. Reactive species ($^1O_2$, $^{\bullet}OH$) were detected by Electron Paramagnetic Resonance (EPR) spectroscopy, with the analysis method provided in Text S2. The concentration of Fe(VI) was measured using UV-Visible spectrophotometry (Shimadzu, Japan) at 510 nm, as described in Text S3. Sulfamethoxazole degradation products were examined using an ultra-high-performance liquid chromatography-quadrupole time-of-flight mass spectrometer (UPLC-QTOF-MS/MS, Agilent 6500), with further details in Text S4 and Table S6. The geometry of pollutants was optimized using Density Functional Theory (DFT) with the Gaussian09 (G09) package at the B3LYP level. The HOMO and LUMO energies were computed employing the 6–311 G(d,p) basis set. Additionally, the 6–31 +G (d,p) basis set was used for further optimization, and the DFT Fukui Function was employed to predict sulfamethoxazole's reactive sites. The analysis of Fe^{2+} concentration in the reaction system and the standard calibration curve are presented in Text S5 and Fig. S1. Methods for monitoring hydrogen peroxide concentration changes are shown in Text S6 and Fig. S2.

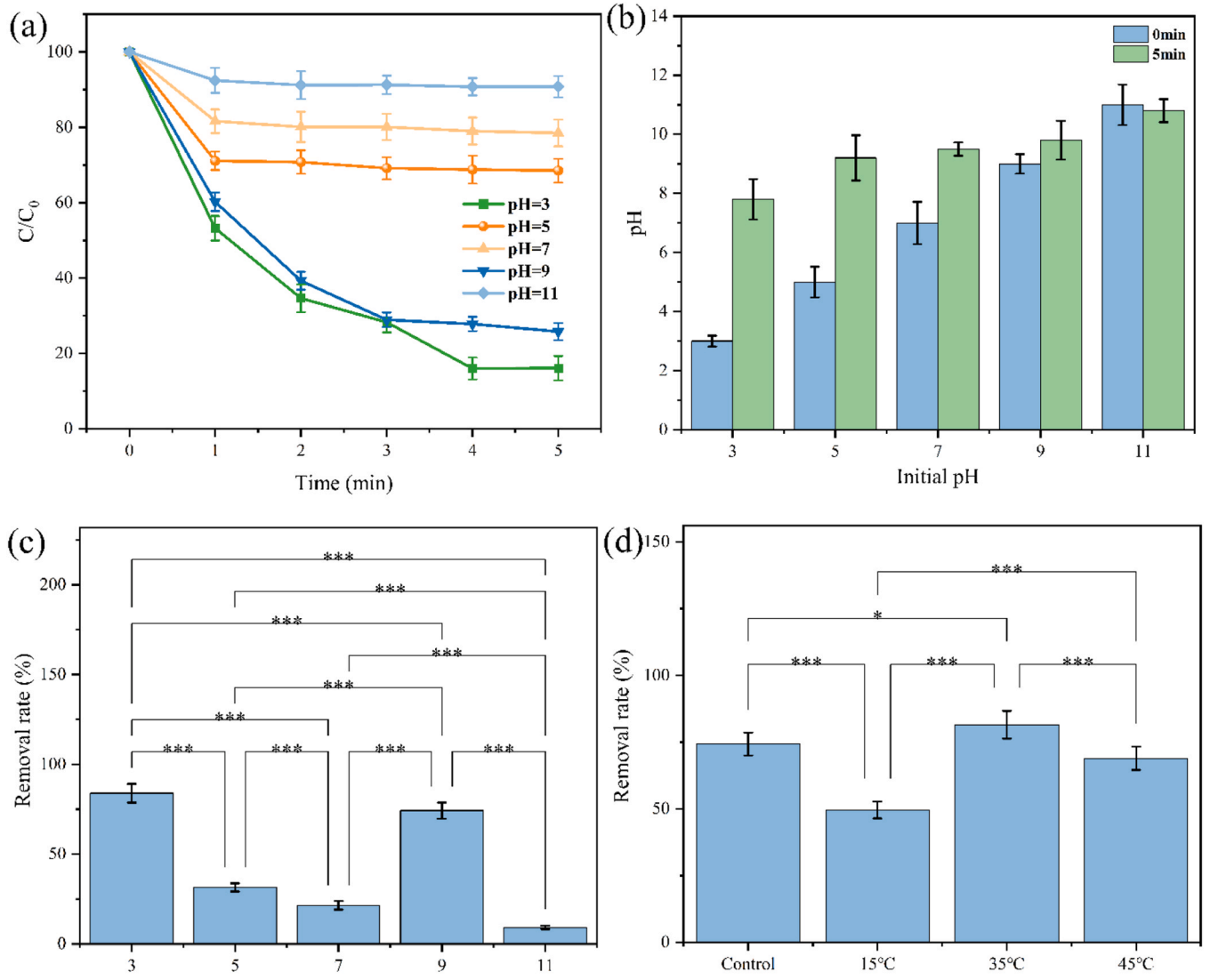

Fig. 2. (a) Removal efficiency of sulfamethoxazole at different pH (b) changes of solution pH before and after sulfamethoxazole removal reaction. (c) Effects of different pH on SMX removal rate at 5 min. (d) Effects of different temperature on SMX removal rate at 5 min. Conditions: [sulfamethoxazole] = 0.02 mM, [Fe(VI)] = 0.4 mM, [$NaBO_3$] = 0.4 mM, pH_0 = 3–11, T = 25°C. "*" represents significant differences in the one-way ANOVA, where "*" means $p \leq 0.05$, "**" means $p \leq 0.01$, and "***" means $p \leq 0.001$.

2.4. Statistical analysis

Analysis of variance (ANOVA) was employed to evaluate the significance of individual factors including ferrate concentration, sodium perborate dosage, pH, and temperature on the degradation efficiency of SMX. A full factorial design was used to systematically investigate both the main effects and potential interactions among the variables. The statistical analysis was conducted using Origin 2024, and a p-value less than 0.05 was considered statistically significant.

2.5. Phytotoxicity test

The phytotoxicity of Trigonella foenum-graecum L. (fenugreek) and Vigna radiata L. (mung bean) was evaluated through seed germination tests. Ten seeds of fenugreek and mung bean were placed on filter paper, and all petri dishes were kept in the dark at 28°C. A seed germination test was conducted in triplicate for each test solution. The test was divided into three groups, with Group A being cultivated using pure water [33]. Group B was cultivated using Fe(VI)/perborate-treated water containing SMX pollutants, while Group C was cultivated using untreated water containing SMX pollutants. After 2 days, the germination rates of fenugreek and mung bean were measured. Seven days after germination, the seedlings were harvested, and the total length was measured [12]. The toxicity risk of SMX degradation products was assessed based on the germination rates of fenugreek and mung bean, as well as the seedling length.

3. Results and discussion

3.1. The study of Fe(VI)/perborate system removal

3.1.1. Removal of Fe(VI)/perborate system for different pollutants

In this study, we initially investigated the degradation of SMX by the Fe(VI)/perborate system, the Fe(VI) system, and the perborate system. As illustrated in Fig. S5, the Fe(VI)/perborate system achieved a removal rate of 74.2 % for SMX within 5 minutes, whereas the addition of Fe(VI) alone resulted in only a 36.25 % removal rate, and the use of perborate alone was almost ineffective in removing SMX. Consequently, the Fe(VI)/perborate system demonstrated a significant advantage over the individual application of Fe(VI) and perborate in degrading SMX. To further explore the degradation capabilities of the Fe(VI)/perborate system on various pollutants, additional experiments were conducted.

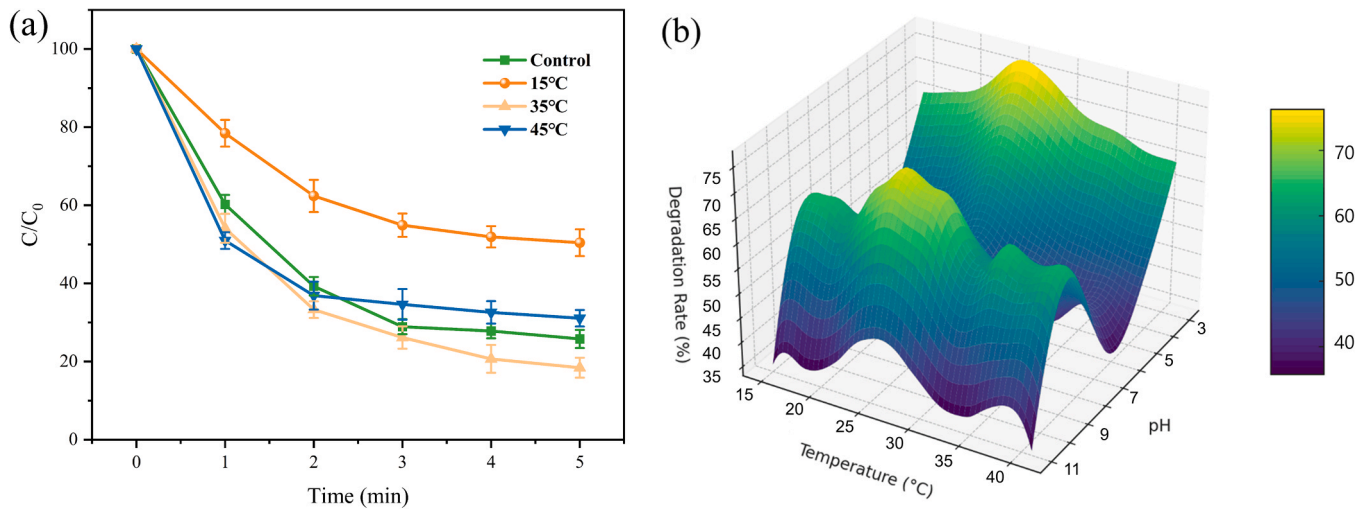

Fig. 3. (a) Removal efficiency of sulfamethoxazole at different temperature, (b) surfaces corresponding to the interaction between temperature and pH. Conditions: [sulfamethoxazole] = 0.02 mM, [Fe(VI)] = 0.4 mM, [$NaBO_3$] = 0.4 mM, pH_0 = 9.2, T = 15–45°C.

This study investigated the removal performance of the Fe(VI)/perborate system for various contaminants, including carbamazepine, ciprofloxacin, tetracycline, amoxicillin, ibuprofen, and metronidazole in the pure water. As shown in Fig. S6, tetracycline achieved a removal rate of 97.34 % within 1 minute, while carbamazepine and amoxicillin reached 100 % removal within 3 minutes. Ciprofloxacin and metronidazole showed removal rates of 89.23 % and 91.67 %, respectively, within 5 minutes. In contrast to the Fe(VI) system by itself, the removal rates of these pollutants were significantly enhanced. However, ibuprofen exhibited a relatively low removal rate of only 13.89 % after 5 minutes. This is likely due to the molecular structure of ibuprofen, which contains an aromatic ring and a carboxyl group [25]. These structural features confer a certain degree of stability in water, and the lack of highly reactive functional groups in ibuprofen contributes to its lower removal efficiency [38].

3.1.2. The concentrations of Fe(VI) and sodium perborate

As shown in Fig. 1a, To investigate the optimal concentrations of Fe (VI) and sodium perborate in the Fe(VI)/perborate, at 0.4 mM, the Fe (VI) concentration was set up. while the sodium perborate concentrations ranged from 0.2 mM to 1.0 mM, with increments of 0.2 mM.

As shown in Fig. 1c and d, Through one-way ANOVA, $p < 0.05$ indicated that perborate and Fe(VI) had significant effects on the removal rate of SMX. With the increase of ferrate and perborate concentration, SMX degradation rate increased significantly, which may be attributed to the enhanced concentration dependence of Fe(VI) oxidizing species, which promoted the direct oxidation of sulfanilamide pollutants or indirect free radical generation. The corresponding removal rates within 5 minutes were 36.01 %, 25.8 %, 43.16 %, 23.76 %, and 44.17 %, respectively. Typically, an increase in activator concentration leads to Fe(VI) changed into Fe(V) and Fe(IV), resulting in higher concentrations of reactive species such as $O_2^{\bullet-}$, $^1O_2$, and $^{\bullet}OH$ in the system. Therefore, the removal rate of sulfamethoxazole increased as the concentration of sodium perborate rose from 0.2 mM to 0.8 mM. However, when the sodium perborate concentration reached 1.0 mM, the removal rate of sulfamethoxazole decreased. This decrease is explained by the fact that with greater concentrations of sodium perborate, although Fe(VI) is more efficiently activated, more amorphous Fe(III) is produced, which reduces the overall removal efficiency of Fe(VI) and sodium perborate towards sulfamethoxazole [2]. As the concentration of sodium perborate in the system increased, the removal rate of sulfamethoxazole rose at the beginning and then fell. Although the removal rate of sulfamethoxazole increased with an increase in sodium perborate concentration from 0.2 mM to 0.8 mM, the difference in the final sulfamethoxazole removal rate after 5 minutes was not significant. Additionally, considering that the removal rate was too high at 0.8 mM sodium perborate, making sampling difficult in the short term and hindering mechanistic studies, the sodium perborate concentration of 0.4 mM was selected for further removal experiments on sulfamethoxazole.

As shown in Fig. 1b and Fig. S7, when the sodium perborate concentration was set at 0.4 mM, the Fe(VI) concentrations were varied at 0.1 mM, 0.2 mM, 0.4 mM, 0.6 mM, and 1.6 mM. It was observed that as an increase in Fe(VI) concentration, the removal rate of sulfamethoxazole gradually increased. Although the removal rate reached 77.86 % within 1 minute at an Fe(VI) concentration of 1.6 mM, the final removal rate after 5 minutes did not show significant improvement. At an Fe(VI) concentration of 0.6 mM, despite a higher reaction rate (7.3159×10^3 $M^{-1}s^{-1}$), the removal rate of sulfamethoxazole after 2 minutes (23.06 %) was not significantly different from that at 0.4 mM Fe(VI) (25.8 %). Therefore, the Fe(VI) concentration of 0.4 mM was selected for further investigation in the reaction system.

3.1.3. Change of initial pH

As shown in Fig. 2c, the ANOVA results indicated that the removal efficiencies of SMX differed significantly under various pH conditions, demonstrating that pH had a statistically significant effect on SMX removal rate. As shown in Fig. 2a, the removal rates of sulfamethoxazole reached 83.9 % and 74.2 % under initial pH conditions of 3 and 9, respectively. This difference in removal efficiency can be clarified by that Fe(VI) exists in the forms of H_2FeO_4, $HFeO_4^-$, $H_3FeO_4^+$, and FeO_4^{2-}, and the redox potential of these species varies under different pH conditions [42]. Density functional theory (DFT) calculations on the Fe(VI) reactive ability with organic compounds indicated that the density of spin charges in oxoligands was higher in $HFeO_4^-$ than in FeO_4^{2-} [37]. Therefore, under acidic conditions, Fe(VI) exhibited a higher removal efficiency for sulfamethoxazole, while the removal rates at pH 5 and pH 7 were 31.5 % and 21.5 %, respectively, lower than the rate at pH 9. This is likely because under neutral and slightly acidic conditions, Fe(VI) is highly unstable and undergoes rapid self-decomposition in the solution, leading to a rapid decrease in the concentrations of the reactive Fe (V)/Fe(IV) species [11]. It is reported that Fe(VI) exhibits excellent oxidation performance in both municipal and industrial wastewater at pH 8–10. When Fe(VI) was applied under alkaline conditions, the removal efficiency of BPA in municipal wastewater reached 90 % [44]. Additionally, after Fe(VI) treatment of medical wastewater under alkaline conditions, the COD value decreased to 21.3 % (Li, J. et al.[14]. A pilot-scale experiment on Fe(VI) treatment of wastewater indicated that

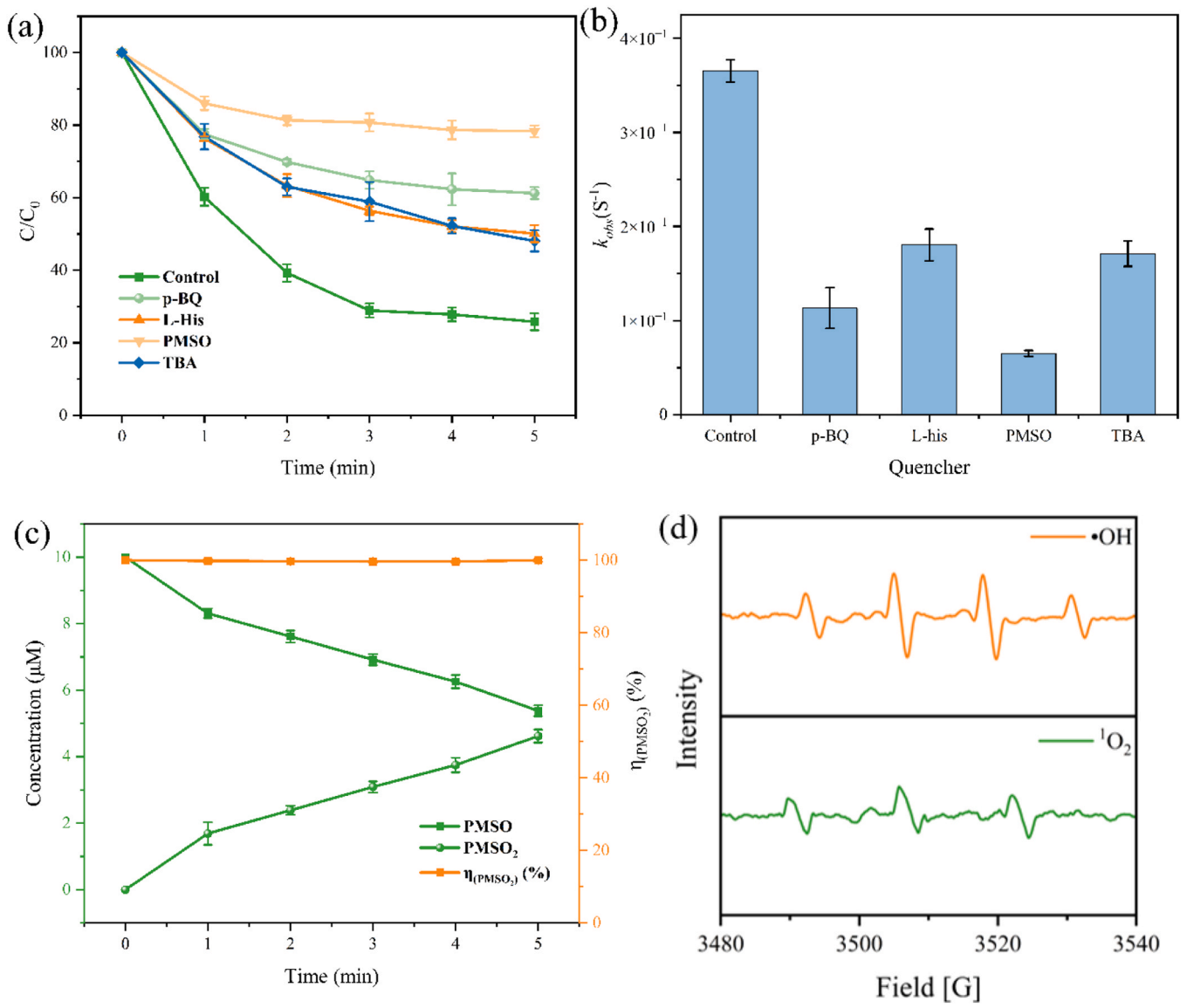

Fig. 4. (a) Effect of quenching experiment on sulfamethoxazole removal; (b) Pseudo-first-order kinetic constant of sulfamethoxazole removal in quenching test; (c) Conversion of PMSO in Fe(VI)/perborate system; (d) EPR analysis of $^{\bullet}OH$ and $^{1}O_2$ radicals of Fe(VI)/perborate system; Conditions: [sulfamethoxazole] = 0.02 mM, [Fe(VI)] = 0.4 mM, [$NaBO_3$] = 0.4 mM, [p-BQ] = 10 mM, [L-his] = 10 mM, [TBA] = 100 mM, [DMPO] = 100 mM, [TEMP] = 20 mM, pH_0 = 9.2, T = 25°C.

the COD value decreased as the initial pH increased, while the pollutant removal rate increased [24]. This is most likely due to acidic conditions, which can lead to the self-decomposition of Fe(VI) [39]. Therefore, under alkaline conditions, the oxidizing power of the Fe(VI)/perborate system can be maximized. Following five minutes of reaction as seen in Fig. 2c, the reaction solution's pH stabilized around 9, which is within the optimal pH range for Fe(VI) degradation. This is ascribed to the buffering effect of H_3BO_3 and $B(OH)_4^-$, which are generated during the activation of Fe(VI) and the hydrolysis of sodium perborate [15]. This buffering capacity helps maintain the oxidative strength of Fe(VI) and facilitates the efficient removal of sulfamethoxazole [5].

3.1.4. Change of temperature

Fig. 3a illustrates the removal rates of sulfamethoxazole were 49.58 %, 81.57 %, and 68.9 % at reaction temperatures of 15°C, 35°C, and 45°C, respectively. As seen in Fig. S8b, the k_{obs} value increased from 0.1993 min^{-1} at 15°C to 0.4543 min^{-1} at 35°C. This increase is due to the accelerated hydrolysis of sodium perborate as the temperature increases, promoting the dissociation of the O-O bonds in HOOBO and $HOOB(OH)_3$, which results in the generation of reactive species such as $^{1}O_2$ and $O_2^{\bullet-}$ Li, S. et al.[16]. This accelerates the activation of Fe(VI) and its transformation into Fe(V)/Fe(IV), thereby improving the removal rate of sulfamethoxazole [52]. However, the removal rate of sulfamethoxazole showed no significant improvement at 45°C. This could be because at higher temperatures, the stability of Fe(V)/Fe(IV) species is compromised, leading to the formation of more amorphous Fe(III), which in turn suppresses sulfamethoxazole degradation [2]. As shown in Fig. 2d, ANOVA analysis demonstrated a significant variation in SMX removal efficiencies across different temperatures. Nevertheless, the difference between 15 °C and 35 °C was comparatively less pronounced, possibly due to the dual regulatory role of temperature in the oxidation process. As shown in Fig. 3b, In this study 3d surface diagram was utilized to analyze and determine the optimal pH and temperature for SMX degradation in the Fe(VI)/perborate system. The results indicated that the highest degradation efficiency was achieved at approximately pH 9 and pH 3, as well as around 25°C, which was consistent with the experimental findings. However, considering that a pH of 3 does not align with most real-world wastewater treatment conditions, pH 9 is more practical for application. Therefore, for subsequent studies, the conditions of pH 9.2 and a temperature of 25°C were chosen to evaluate

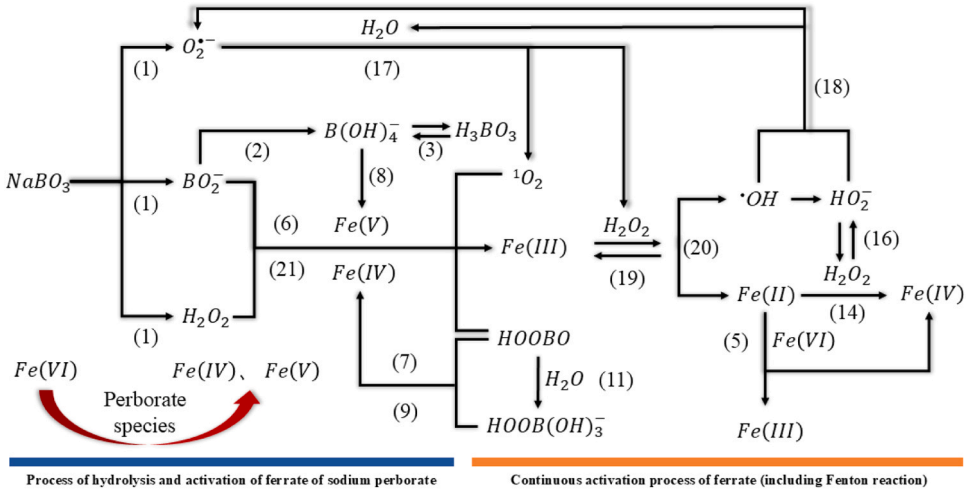

Fig. 5. The main mechanism of sulfamethoxazole removal by Fe(VI)/perborate system.

the Fe(VI)/perborate system's removal efficiency for sulfamethoxazole.

3.2. Study on reaction mechanism of Fe(VI)/perborate system

3.2.1. The determination of active substance

It's reported that after the hydrolysis of sodium perborate, the peroxide O-O bonds in sodium perborate break, resulting in the formation of $O_2^{\bullet-}$ [49]. The sufficient amount of $O_2^{\bullet-}$ generated by the hydrolysis of sodium perborate ensures the enhanced activation of Fe(VI), accelerating its conversion to Fe(V) and Fe(IV). To determine the contribution of reactive species in the Fe(VI)/perborate system, p-Benzoquinone (p-BQ), L-Histidine (L-His), and Tert-butanol (TBA) were used to quench the reactive species $O_2^{\bullet-}$, $^1O_2$, and $^{\bullet}OH$. The reaction rate constant has been found that between p-BQ and $O_2^{\bullet-}$ is as high as 1.0×10^9 $M^{-1}s^{-1}$ [8]. The reaction rate constant for L-His and $^1O_2$ is 3.2×10^7 $M^{-1}s^{-1}$ [3]. The rate constant for TBA and •OH ranges from (3.8–7.6) $\times 10^8$ $M^{-1}s^{-1}$ [19]. When 10 mM p-BQ, L-His, and 100 mM TBA were incorporated into the solution, the sulfamethoxazole removal rates decreased to 38.73 %, 49.9 %, and 51.91 %, respectively, as shown in Fig. 4b, indicating substantial suppression of sulfamethoxazole removal. As shown in Fig. 4c, the reaction rate constants dropped from 0.36530 $M^{-1}s^{-1}$ in the control group to 0.11329 $M^{-1}s^{-1}$, 0.18049 $M^{-1}s^{-1}$, and 0.17115 $M^{-1}s^{-1}$ with the addition of the quenching agents. This decrease suggests that the system's reactive species was effectively suppressed by the quenching agents. These results provide preliminary evidence for the involvement of $O_2^{\bullet-}$, $^1O_2$, and $^{\bullet}OH$ in the Fe(VI)/perborate system.

PMSO is a probe contaminant used to detect the presence of Fe(IV)/Fe(V) [56]. The reaction between Fe(V)/Fe(IV) and PMSO proceeds via a $2e^-$ transfer mechanism, ultimately resulting in PMSO conversion to $PMSO_2$. The reaction rate between PMSO and Fe(IV)/Fe(V) has been reported to be 2.58×10^3 $M^{-1}s^{-1}$ [27,56]. This confirms Fe(IV)/Fe(V) in the Fe(VI)/perborate system and their role in sulfamethoxazole removal. As shown in Fig. 4a and b, the sulfamethoxazole removal rate reduced from 74.2 % to 21.67 % after the PMSO addition and the rate of reaction dropped from 0.3653 to 0.0652. The preferential reaction between Fe(V)/Fe(IV) and PMSO leads to the inhibition of sulfamethoxazole removal [51]. As shown in Fig. 4c, after the addition of PMSO, the conversion rate of PMSO to $PMSO_2$ reached nearly 100 %. This indicates that the influence of other reactive species in the system can be neglected and confirms that Fe(IV)/Fe(V) is the dominant reactive species responsible for sulfamethoxazole removal.

Reactive oxygen species were identified using EPR in the Fe(VI)/perborate system, with DMPO and TEMP serving as spin traps for $^{\bullet}OH$ and $^1O_2$, respectively. Fig. 4d shows the successful detection of typical signals for TEMPO-$^1O_2$ adducts (1:1:1) in the Fe(VI)/perborate system (Fig. 4a), confirming the generation of $^1O_2$. Additionally, The DMPO--$^{\bullet}OH$ signal was observed, confirming the presence of both of these reactive species.

3.2.2. Mechanism of reaction in the Fe(VI)/perborate system

The Fe(VI)/perborate system consists of two main components: (1) $NaBO_3$ accelerates Fe(VI) activation, and (2) the fenton reaction and subsequent continuous activation processes. Studies have shown that $NaBO_3$, when dissolved in water, hydrolyzes to produce $O_2^{\bullet-}$, BO_2^-, and H_2O_2 [17,54]. As shown in Fig. 5, BO_2^- further hydrolyzes to form $B(OH)_4^-$. The species $B(OH)_4^-$, H_2O_2, and BO_2^- can interact with Fe(V) and Fe(IV) to generate $^1O_2$, thereby increasing the number of system's reactive oxygen species. As shown in Eq. 22–24, $B(OH)_4^-$ and BO_2^- can accelerate the Fe(VI) reduction to Fe(V) and Fe(IV), ensuring the rapid activation of Fe(VI) in a short time and significantly enhancing the oxidative power of the system. Ultimately, Fe(VI) is converted to Fe(III), and under the combined effect of H_2O_2 produced during the initial hydrolysis of $NaBO_3$ and the self-decomposition of ferrate, as shown in Eq. 20, Fe(III) reacts with H_2O_2 to generate $^{\bullet}OH$ and Fe(II). The resulting Fe(II) can then undergo the Fenton reaction with H_2O_2, ensuring the sustained oxidative capacity of the system [41]. This is also the reason why the Fe(VI)/perborate system significantly improves the sulfamethoxazole removal efficiency compared to using ferrate alone. As shown in Eq. 16, the HO_2^- produced from the hydrolysis of H_2O_2 reacts with the generated $^{\bullet}OH$ to form $O_2^{\bullet-}$, enriching the system with various reactive oxygen species and enhancing its oxidative power. Additionally, as shown in Eq. 14, H_2O_2 reacts with Fe(II) to reduce it to Fe(IV), ensuring that Fe(IV) and Fe(V) are present in sufficient concentrations within the system. This is consistent with Fig. S2, where Fe(III) interacts with H_2O_2 to raise the concentration of Fe(II). Later, with the occurrence of the Fenton reaction and the reaction between Fe(II) and Fe(VI), part of Fe(II) is converted to Fe(III), leading to a brief drop in the concentration of Fe(II). The acceleration of Fe(VI) activation to Fe(V) and Fe(IV) by $NaBO_3$ hydrolysis products, along with the Fenton reaction mechanisms in the second phase, significantly enhances the oxidative capacity of the solution within a certain period, ensuring the efficient removal of sulfamethoxazole.

3.3. Study on anti-interference ability of Fe(VI)/perborate system

3.3.1. Effects of inorganic anions and humic acids

To assess the Fe(VI)/perborate system's ability to withstand interference, the effects of various concentrations (1 mM and 5 mM) of Cl^-, CO_3^{2-}, HCO_3^-, SO_4^{2-}, as well as humic acid (HA) concentrations of 10 mg/L and 40 mg/L, on the impact of sulfamethoxazole removal was studied.

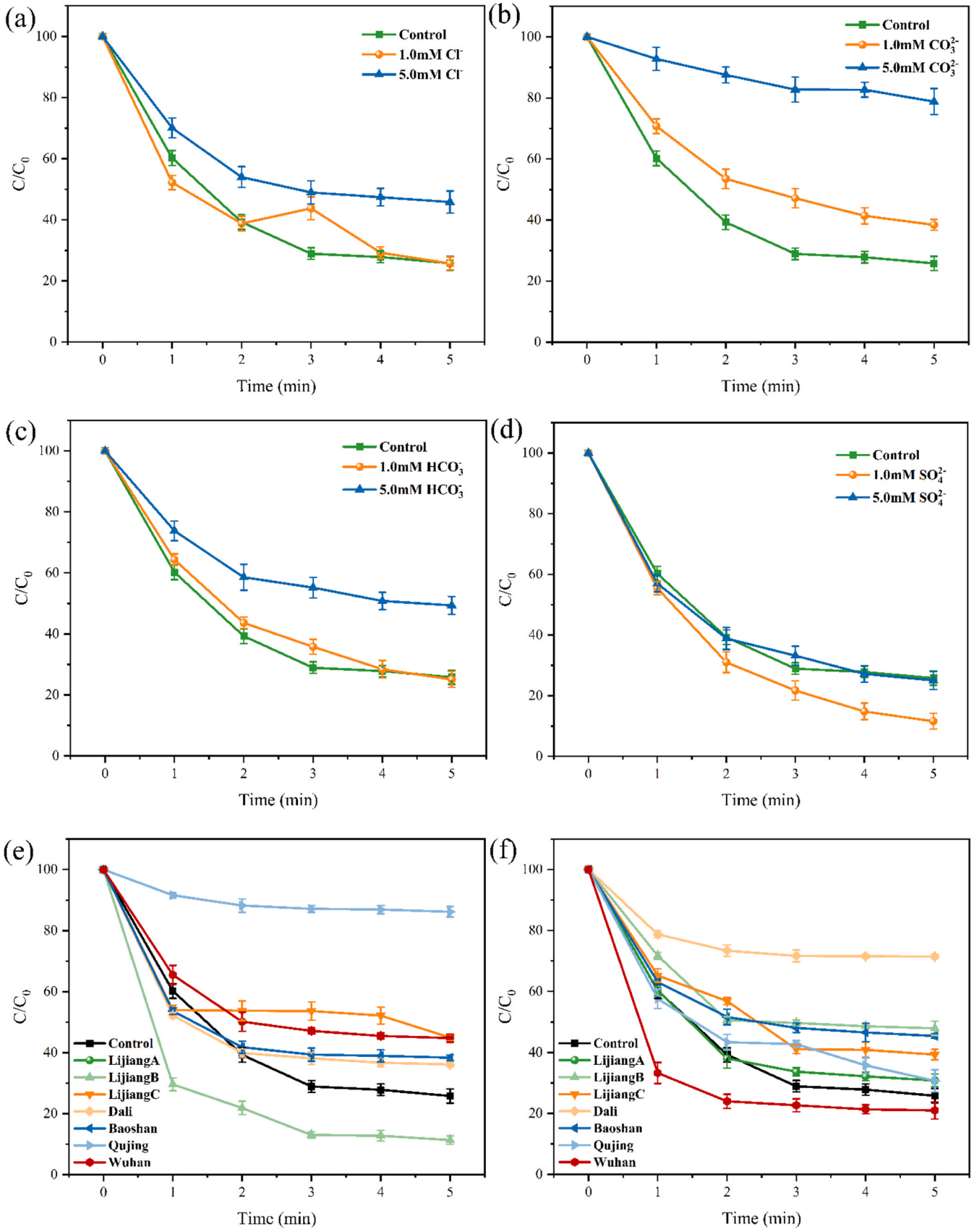

Fig. 6. Experimental effect of inorganic anion on sulfamethoxazole removal (a) Cl^-, and (b) CO_3^{2-}, and (c) HCO_3^-, and (d) SO_4^{2-}; Removal efficiency of sulfamethoxazole in actual WWTP water treatment (e) influent, and (f) effluent. Conditions: [sulfamethoxazole] = 0.02 mM, [Fe(VI)] = 0.4 mM, [$NaBO_3$] = 0.4 mM, [Cl^-] = [CO_3^{2-}] = [HCO_3^-] = [SO_4^{2-}] = 1 mM, 5 mM, pH_0 = 9.2, T = 25°C.

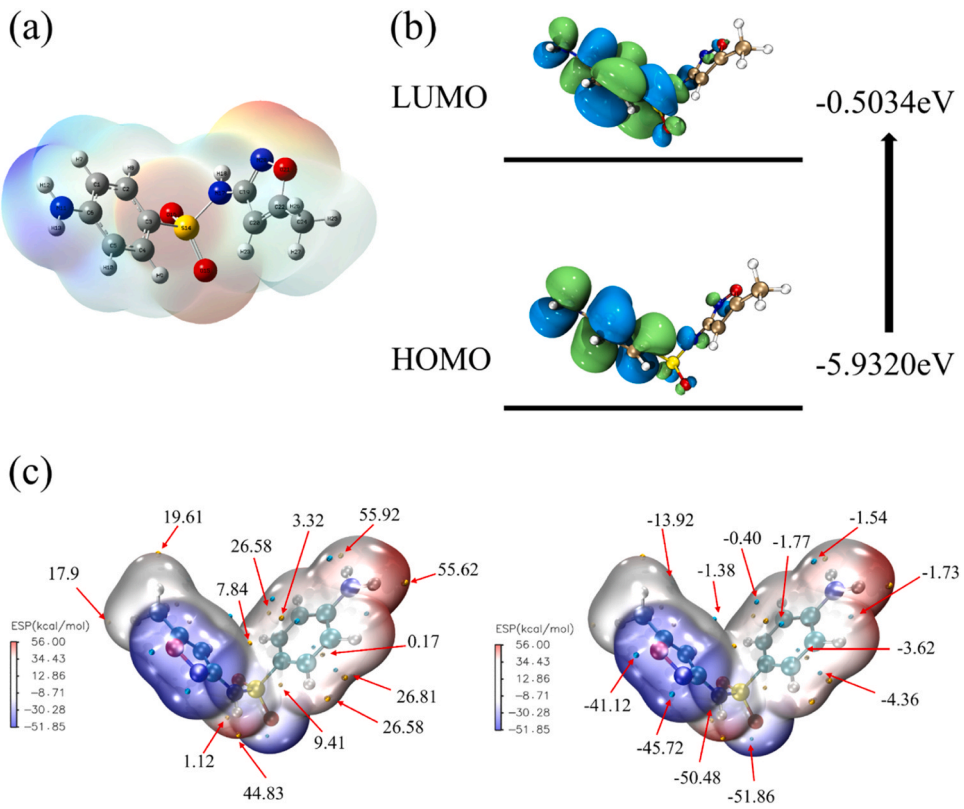

Fig. 7. (a) The electrostatic potential energy diagram of sulfamethoxazole. (b) LUMO and HOMO orbit of sulfamethoxazole. (c) SMX molecular surface electrostatic potential and the distribution of the extreme value point.

As shown in Fig. 6d, SO_4^{2-} had minimal impact on the Fe(VI)/perborate system. In fact, at a SO_4^{2-} concentration of 1 mM, the sulfamethoxazole removal rate (88.41 %) was higher than that observed without SO_4^{2-} (74.2 %), demonstrating that the Fe(VI)/perborate system has good tolerance to SO_4^{2-} in aqueous solutions. In contrast, the addition of 5 mM CO_3^{2-} and HCO_3^- greatly reduced sulfamethoxazole removal, with removal rates dropping to 21.2 % and 50.64 %, respectively. The CO_3^{2-} and HCO_3^- hydrolysis may be the cause of this phenomenon, leading to a slightly alkaline aqueous solution and thereby suppressing the generation of active substances. However, when 1 mM CO_3^{2-} and HCO_3^- were added, the impact on sulfamethoxazole removal was less significant, with removal rates of 61.58 % and 74.9 %, respectively. This phenomenon can be clarified by the buffering effect of borates generated in the Fe(VI)/perborate system, which helps maintain the pH stability of the reaction solution, ensuring efficient sulfamethoxazole removal. The addition of 5 mM Cl^- also inhibited the removal of sulfamethoxazole, reducing the reaction rate constant k_{obs} from 0.3650 min^{-1} to 0.2461 min^{-1} . As shown in Fig. S11, HA caused significant interference in the Fe(VI)/perborate system, with the sulfamethoxazole removal rate dropping to 42.75 % and 38.75 % after 5 minutes, and k_{obs} decreasing to 0.1425 min^{-1} and 0.1160 min^{-1} , respectively. Previous studies have indicated that HA can scavenge active radicals in the reaction system, competing with sulfamethoxazole for these radicals, thereby inhibiting sulfamethoxazole removal [22].

3.3.2. Study on actual sewage treatment

Fe(VI) is unstable in water and tends to decompose rapidly, which poses a challenge for its practical application in wastewater treatment. Since Fe(VI) is typically introduced during the pretreatment and advanced treatment stages of actual wastewater treatment, the Fe(VI)/perborate system's sulfamethoxazole removal effectiveness was assessed in WWTP influent and secondary effluent. As shown in Fig. 6e, the sulfamethoxazole removal rate in the influent of the WWTPs ranged from 13.85 % to 88.63 %, with the exception of Lijiang B, where the removal rate was lower than that observed in pure water. The removal rates in Lijiang A, Lijiang C, Dali, Baoshan, Qujing, and Wuhan were 53.24 %, 55.05 %, 63.89 %, 61.65 %, 13.85 %, and 35.52 %, respectively. The removal efficiency of SMX in sewage is lower than that in pure water, probably because the actual sewage contains rich organic substances and ions, which consumes part of active free radicals, resulting in insufficient overall oxidation [47]. As shown in Table S1, the lowest removal rate was observed at Qujing WWTP, likely due to the significantly higher COD and NH_3-N content in the influent, which may compete with sulfamethoxazole for active radicals. In this case, appropriately increasing the ratio of Fe(VI) to perborate will enhance the removal efficiency of SMX [48]. In the WWTP effluent, the sulfamethoxazole removal rates for Lijiang A, Lijiang B, Lijiang C, Dali, Baoshan, Qujing, and Wuhan were 69.17 %, 52.08 %, 60.69 %, 28.53 %, 54.58 %, 69.28 %, and 79 %, respectively. The low removal rate in Dali WWTP may be attributed to the higher T-N content (12.1 mg/L) in the water compared to Wuhan WWTP (8.2 mg/L), which could interfere with the active radicals in the reaction system. As shown in Fig. S13, the removal rate constants k_{obs} for sulfamethoxazole in Lijiang A, Lijiang B, Lijiang C, Dali, Baoshan, Qujing, and Wuhan were 0.4427 min^{-1} , 0.2298 min^{-1} , 0.3209 min^{-1} , 0.1487 min^{-1} , 0.2706 min^{-1} , 0.2558 min^{-1} , and 0.6642 min^{-1} , respectively. Despite the variations in water quality, sulfamethoxazole was still effectively removed in these real-world wastewater samples, indicating that the Fe(VI)/perborate system demonstrates excellent interference resistance and holds great potential for practical applications in advanced wastewater treatment.

3.4. Sulfamethoxazole degradation toxicity analysis

As shown in Fig. 7c, the distribution of the extreme points of the SMX molecule is presented, along with a visual analysis of its electrostatic potential. The molecule's central and upper regions appear in red,

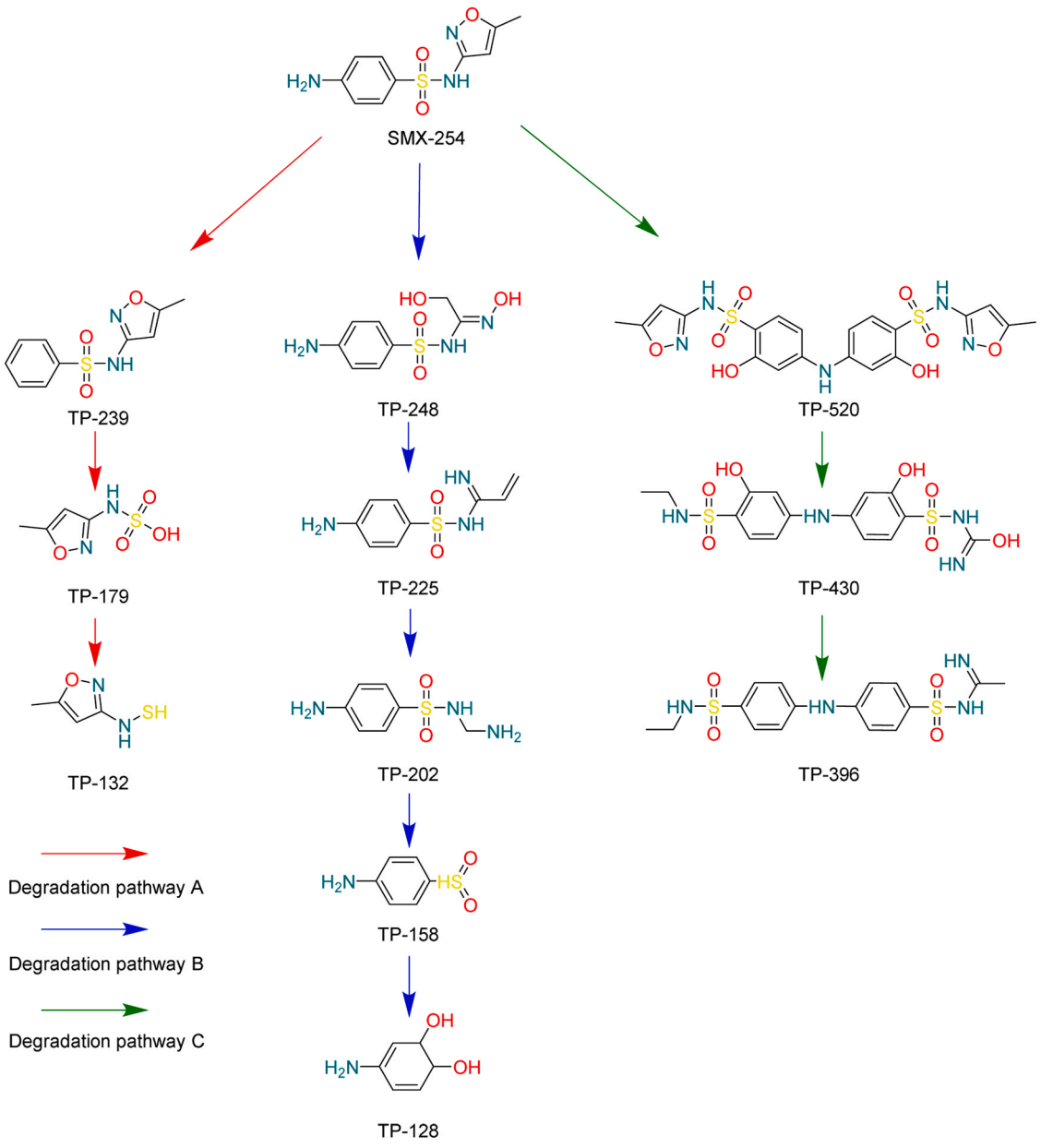

Fig. 8. Possible degradation pathways of sulfamethoxazole.

indicating areas with high negative charge density, with the minimum negative charge of −51.86 kcal/mol, while the blue regions represent areas with positive charge density with the maximum negative charge of 55.92 kcal/mol. Fe(VI) typically attacks regions with high negative charge density, suggesting that SMX degradation initiates in the regions of higher negative charge density where bond cleavage occurs. The regions of high positive charge density, due to their low electron density, are generally not preferred attack sites for active free radicals. However, as the degradation process progresses and the SMX structure breaks down, the resulting small molecules, being unstable, may become susceptible to attacks by $^{\bullet}$OH and Fe(VI).

As shown in Fig. 8b, and Table S6, The HOMO of SMX is primarily located on the benzene ring, nitrogen atom, and sulfur atom. It is reported that the oxidation of SMX by Fe(VI) mainly occurs at the isoxazole and aniline moieties [34]. DFT calculations revealed that the f-values for 11(N) and 14(S) are 0.1081 and 0.0923, respectively, with f0 for 11(N) being 0.0827, all of which are at their highest values. This indicates that 11(N) and 14(S) are highly susceptible to attack by reactive oxygen species. As shown in Fig. 8a, SMX exhibit a high negative charge density in their central regions and a high positive charge density in their peripheral regions. The C═O group, with an electron density of −2.30 eV, acts as a Lewis basic site due to its lone electron pairs. This indicates that the enhanced electron density of the C═O group and its surrounding regions facilitates electron transfer to Fe(VI), thereby promoting the generation of reactive species. LC-MS analysis of the degradation products of sulfamethoxazole identified possible degradation pathways and corresponding products. Products of degradation with values of *m/z* greater than 254 are primarily composed of the sulfamethoxazole molecule and its by-products, as depicted in degradation pathways C [31]. Reactive oxygen species typically attack regions with negatively charged groups, high HOMO orbitals, and elevated f0 and f- values. In the case of sulfamethoxazole, the amine group is targeted, resulting in the generation of degradation products TP-520 through re-association. Concurrently, electrophilic substitution takes place on the aromatic ring, resulting in the formation of ortho-hydroxy TP-430. Subsequent cleavage products undergo

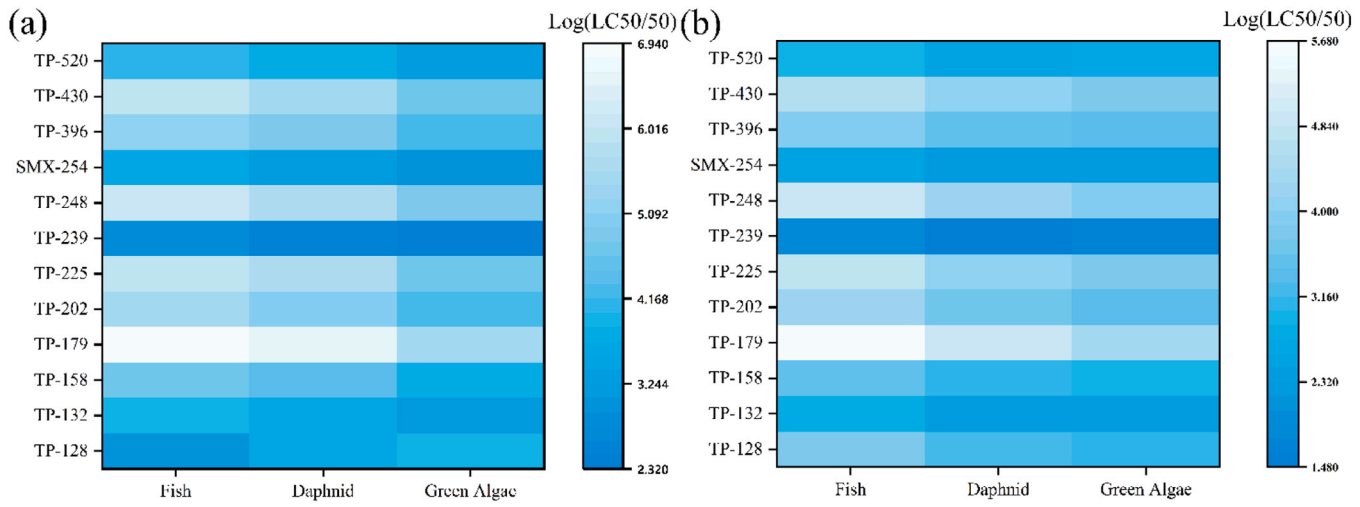

Fig. 9. Acute(a), and chronic(b) toxicity heat maps of sulfamethoxazole degradation products.

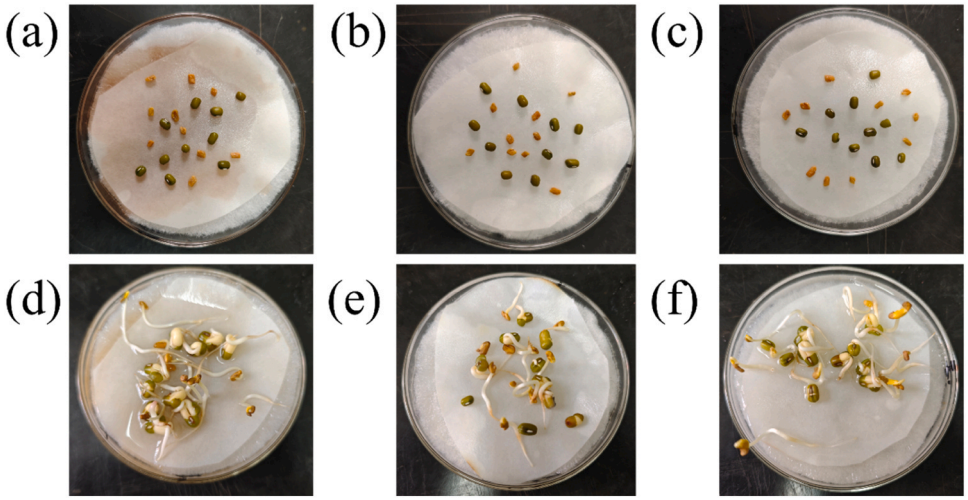

Fig. 10. On day 0, (a) Fe(VI)/perborate treatment hydroponics, (b) 0.02 mM SMX hydroponics, (c) pure water hydroponics (Control); on day 7, (a) Fe(VI)/perborate treatment hydroponics, (b) 0.02 mM SMX hydroponics, (c) pure water hydroponics (Control).

dehydroxylation, yielding TP-396. In degradation pathway B, $^{\bullet}OH$ attacks the carbon atom adjacent to the amine group, leading to hydroxylation of sulfamethoxazole, producing TP-248, which is further oxidized to form TP-202 [18]. This cleavage site is also consistent with the vulnerable sites predicted by DFT calculations, and the degradation product analysis by LC-MS confirmed the previous predictions from DFT calculations. Subsequently, the S-N bond breaks, leading to the creation of the sulfonic acid byproduct TP-158, which is eventually oxidized to TP-128 [30]. In degradation pathway A, the reactive oxygen species $^1O_2$ attacks the S═O bond in TP-179, undergoing an aminolysis reaction to form TP-132 [1]. Ultimately, all degradation products continue to oxidize, breaking down into smaller fragments, which are mineralized to generate H_2O and CO_2 [20].

3.5. Toxicity assessment of SMX degradation products

As shown in Table S8 and Fig. 9, to further assess the level of toxicity of the degradation products during sulfamethoxazole removal. The study applied ECOSAR v2.2 to forecast both acute and chronic toxicity of sulfamethoxazole and its byproducts to fish, water fleas, and algae. The results confirmed that, except for the macromolecular degradation products such as TP-520, TP-430, the acute toxicity of other small molecule degradation products generally decreased. Notably, both the acute and chronic toxicity level of TP-128 and TP-239 were lower than that of the parent sulfamethoxazole. Studies have reported that TP-179 and TP-239 have no inhibitory effect on the growth of *Escherichia coli* [1]. The oxidation products of SMX, TP-254 and TP-225, have a promotive effect on wheat growth. Within 7 days, the wheat length increased by 2.1 cm compared to those grown in SMX aqueous solution [50]. However, the presence of certain macromolecular products led to an increase in the toxicity of the degradation mixture. Future studies should pay more attention to the toxicity changes associated with these large molecular degradation products.

As shown in Table S9 and Fig. 10, fenugreek and mung bean were cultivated with Fe(VI)/perborate-treated water, 0.02 mM SMX aqueous solution, and pure water, respectively. On the second day, the germination rate of fenugreek in Group A was 100 %, while the germination rate of mung bean was 10 %. In Group B, the germination rate of fenugreek was 90 %, and that of mung bean was 20 %. In Group C, the germination rate of fenugreek was 90 %, and that of mung bean was 20 %. This may be due to the toxicity inherent in SMX, which caused the low germination rate of mung bean. On day 7, the average seedling length of mung bean and fenugreek in Group A was 1.45 cm and 4.1 cm, respectively. On day 7, the average seedling length of mung bean and

fenugreek in Group B was 1.86 cm and 4.2 cm, respectively. On day 7, the average seedling length of mung bean and fenugreek in Group C was 0.83 cm and 2.19 cm, respectively. The untreated SMX-containing aqueous solution significantly inhibited the growth of mung bean and fenugreek. However, the average seedling length of mung bean and fenugreek cultivated with Fe(VI)/perborate-treated water even surpassed that of the pure water-grown mung bean and fenugreek, which is consistent with the predicted reduction in toxicity of SMX degradation products. This may be due to the promoting effect of SMX degradation products TP-254 and TP-225 on the growth of fenugreek and mung bean [50].

4. Conclusion

This study was the first to propose the Fe(VI)/perborate oxidation technique for water treatment.

The Fe(VI)/perborate system is enhanced by borate radicals produced by sodium perborate hydrolysis, which accelerates the activation of Fe(VI) and leads to the formation of large amounts of Fe(V) and Fe (IV). In contrast to Fe(VI) alone to degrade sulfamethoxazole, the Fe (VI)/perborate system generates Fe^{2+}, which further participates in a Fenton reaction with the H_2O_2 produced by perborate, enhancing the system's oxidative capacity. It has been confirmed that the continuous production of borates in the Fe(VI)/perborate system maintains the reaction environment at approximately pH 9, allowing for the best possible oxidation capacity of Fe(VI). Moreover, the H_2O_2 generated within the Fe(VI)/perborate system ensures the sustained oxidative performance of the system. In wastewater from seven different regional treatment plants, both influent and secondary effluent, the Fe(VI)/perborate system demonstrated high efficiency in removing sulfamethoxazole, highlighting its significant potential for practical applications in wastewater treatment. The Fe(VI)/perborate system also demonstrated strong removal efficiency for various pollutants such as tetracycline, carbamazepine, ciprofloxacin, amoxicillin, and metronidazole, offering promising potential for the removal of other contaminants as well.

Environmental implication

This study investigates the degradation of the antibiotic sulfamethoxazole using a ferrate(VI)/perborate system, and evaluates the degradation efficiency of sulfamethoxazole in the influent and secondary effluent of seven wastewater treatment plants. Notably, the ferrate(VI)/perborate system achieves significantly higher removal efficiency for sulfamethoxazole compared to ferrate alone. Additionally, the buffering effect of sodium perborate greatly suppresses the self-decomposition of ferrate, thus preserving the system's oxidation capacity. This study aims to provide a new perspective on antibiotic degradation and the application of ferrate in water treatment, with the goal of further advancing the use of ferrate in water treatment processes.

CRediT authorship contribution statement

Chen Zihe: Writing – review & editing, Writing – original draft, Investigation, Formal analysis, Data curation. **Su Jingzhen:** Formal analysis, Data curation. **Li Cong:** Writing – review & editing, Supervision, Project administration, Formal analysis, Data curation, Conceptualization. **Guan Xiaohong:** Formal analysis. **Xu Jiani:** Investigation. **He Zhenming:** Data curation. **Kim Hyunook:** Writing – review & editing. **Bian Yulin:** Investigation.

Ethical approval

The authors mentioned in the manuscript have agreed to authorship, read and approved the manuscript and given consent for submission and subsequent publication of the manuscript.

Declaration of Competing Interest

The authors declare that they have no known competing financial interests or personal relationships that could have appeared to influence the work reported in this paper.

Acknowledgement

This work was sponsored by the National Natural Science Foundation of China (Project No. 52442006) and Project Sponsored by Science and Technology Commission of Shanghai Municipality (Project No. 24DZ2306400). H. Kim is supported by the Korea Environment Industry & Technology Institute (KEITI) through the project for developing innovative drinking water and wastewater technologies funded by Korea Ministry of Environment (MOE) (NO. 2019002710006) and MOE's Graduate School Specialized in Climate Change.

Appendix A. Supporting information

Supplementary data associated with this article can be found in the online version at doi:10.1016/j.jhazmat.2025.138261.

Data Availability

Data will be made available on request.

References

[1] Akbari, M.Z., Xu, Y., Liang, C., Lu, Z., Shen, S., Peng, L., 2023. Synthesis of ZnO@VC for enhancement of synergic photocatalytic degradation of SMX: toxicity assessment, kinetics and transformation pathway determination. Chem Eng Process - Process Intensif 193, 109544. https://doi.org/10.1016/j.cep.2023.109544.

[2] Bzdyra, B.M., Spellman, C.D., Jr, Andreu, I., Goodwill, J.E., 2020. Sulfite activation changes character of ferrate resultant particles. Chem Eng J 393. https://doi.org/10.1016/j.cej.2020.124771.

[3] Che, M., Xiao, J., Shan, C., Chen, S., Huang, R., Zhou, Y., Cui, M., Qi, W., Su, R., 2023. Efficient removal of chloroform from groundwater using activated percarbonate by cellulose nanofiber-supported Fe/Cu nanocomposites. Water Res 243. https://doi.org/10.1016/j.watres.2023.120420.

[4] Chen, Z., Xu, J., Li, C., Su, J., Bian, Y., Kim, H., Lu, J., 2025. COVID-19 drugs: A critical review of physicochemical properties and removal methods in water. J Environ Chem Eng 13 (1), 115310. https://doi.org/10.1016/j.jece.2025.115310.

[5] Dong, F., Fu, C., Feng, M., Wang, D., Song, S., Li, C., Lichtfouse, E., Li, J., Lin, Q., Sharma, V.K., 2024. Simultaneous generation of free radicals, Fe(IV) and Fe(V) by ferrate activation: a review. Chem Eng J 481, 148669. https://doi.org/10.1016/j.cej.2024.148669.

[6] Fan, W.-Y., Zhang, X., Guo, P.-C., Sheng, G.-P., 2023. Highly efficient removal of phosphonates by ferrate-induced oxidation coupled with in situ coagulation. J Hazard Mater 451. https://doi.org/10.1016/j.jhazmat.2023.131104.

[7] Feng, M., Cizmas, L., Wang, Z., Sharma, V.K., 2017. Synergistic effect of aqueous removal of fluoroquinolones by a combined use of peroxymonosulfate and ferrate (VI). Chemosphere 177, 144–148. https://doi.org/10.1016/j.chemosphere.2017.03.008.

[8] Gao, L., Guo, Y., Zhan, J., Yu, G., Wang, Y., 2022. Assessment of the validity of the quenching method for evaluating the role of reactive species in pollutant abatement during the persulfate-based process. Water Res 221. https://doi.org/10.1016/j.watres.2022.118730.

[9] Goebel, A., McArdell, C.S., Joss, A., Siegrist, H., Giger, W., 2007. Fate of sulfonamides, macrolides, and trimethoprim in different wastewater treatment technologies. Sci Total Environ 372 (2-3), 361–371. https://doi.org/10.1016/j.scitotenv.2006.07.039.

[10] Huang, Z.-S., Wang, L., Liu, Y.-L., Zhang, H.-Y., Zhao, X.-N., Bai, Y., Ma, J., 2021. Ferrate self-decomposition in water is also a self-activation process: Role of Fe(V) species and enhancement with Fe(III) in methyl phenyl sulfoxide oxidation by excess ferrate. Water Res 197, 117094. https://doi.org/10.1016/j.watres.2021.117094.

[11] Huang, Z.-S., Wang, L., Liu, Y.-L., Zhang, H.-Y., Zhao, X.-N., Bai, Y., Ma, J., 2021. Ferrate self-decomposition in water is also a self-activation process: Role of Fe(V) species and enhancement with Fe(III) in methyl phenyl sulfoxide oxidation by excess ferrate. Water Res 197. https://doi.org/10.1016/j.watres.2021.117094.

[12] Kumar, R., Maurya, A., Raj, A., 2024. Exploring the potential of bacterial consortium for the treatment of paper mill effluent treatment through various treatment strategies and evaluation of their toxicity. J Water Process Eng 60. https://doi.org/10.1016/j.jwpe.2024.105135.

[13] Li, C., Li, X.Z., Graham, N., 2005. A study of the preparation and reactivity of potassium ferrate. Chemosphere 61 (4), 537–543. https://doi.org/10.1016/j.chemosphere.2005.02.027.

[14] Li, J., Du, Y., Zhao, E.-Y., Jiang, Y., Wang, Z., Zhang, H., Zhou, P., Xiong, Z., Lai, B., 2023. Enhanced purification of hospital wastewater by a novel ferrate(VI) flocs recycling process. Chem Eng J 461, 141832. https://doi.org/10.1016/j.cej.2023.141832.
[15] Li, J., Prasse, C., Zhang, Z., Hua, Z., Chen, C., Zheng, S., Dong, Z., Fang, J., 2024. Borate buffer significantly alters the formation of cis-2-butene-1,4-dial and chlorinated DBPs during chlorination of phenol. Chem Eng J 495, 153701. https://doi.org/10.1016/j.cej.2024.153701.
[16] Li, S., Zou, J., Li, J., Huang, Y., Wu, J., Wu, Z., Li, Q., Zeng, H., Ma, J., 2024. Strong enhancement on acetaminophen elimination and effective control of chlorinated/brominated by-products generation in heat/ peroxymonosulfate system with sodium perborate. Chem Eng J 496. https://doi.org/10.1016/j.cej.2024.154052.
[17] Li, S., Zou, J., Li, J., Huang, Y., Wu, J., Wu, Z., Li, Q., Zeng, H., Ma, J., 2024. Strong enhancement on acetaminophen elimination and effective control of chlorinated/brominated by-products generation in heat/peroxymonosulfate system with sodium perborate. Chem Eng J 496, 154052. https://doi.org/10.1016/j.cej.2024.154052.
[18] Li, X., Wen, X., Lang, J., Wei, Y., Miao, J., Zhang, X., Zhou, B., Long, M., Alvarez, P. J.J., Zhang, L., 2023. CoN1O2 single-atom catalyst for efficient peroxymonosulfate activation and selective cobalt(IV)=O generation. Angew Chem-Int Ed. https://doi.org/10.1002/anie.202303267.
[19] Li, Y., Dong, H., Li, L., Xiao, J., Xiao, S., Jin, Z., 2021. Efficient degradation of sulfamethazine via activation of percarbonate by chalcopyrite. Water Res 202. https://doi.org/10.1016/j.watres.2021.117451.
[20] Li, Y., Zhao, X., Yan, Y., Yan, J., Pan, Y., Zhang, Y., Lai, B., 2019. Enhanced sulfamethoxazole degradation by peroxymonosulfate activation with sulfide-modified microscale zero-valent iron (S-mFe0): performance, mechanisms, and the role of sulfur species. Chem Eng J 376. https://doi.org/10.1016/j.cej.2019.03.178.
[21] Luongo, G., Previtera, L., Ladhari, A., Di Fabio, G., Zarrelli, A., 2020. Peracetic Acid vs. Sodium Hypochlorite: Degradation and Transformation of Drugs in Wastewater. Molecules 25 (10). https://doi.org/10.3390/molecules25102294.
[22] Lutze, H.V., Bircher, S., Rapp, I., Kerlin, N., Bakkour, R., Geisler, M., von Sonntag, C., Schmidt, T.C., 2015. Degradation of chlorotriazine pesticides by sulfate radicals and the influence of organic matter. Environ Sci Technol 49 (3), 1673–1680. https://doi.org/10.1021/es503496u.
[23] Manoli, K., Li, R., Kim, J., Feng, M., Huang, C.-H., Sharma, V.K., 2022. Ferrate(VI)-peracetic acid oxidation process: Rapid degradation of pharmaceuticals in water. Chem Eng J 429, 132384. https://doi.org/10.1016/j.cej.2021.132384.
[24] Masoumi, H., Nematollahi, D., Talebi, S.M., Karami, F., Nematollahi, P., Pakizeh, S., Talebi, M.R., Torabi, M., Tavakoli, E., Sepehrmansourie, H., 2024. Electrosynthesis of ferrate solution using a novel pilot-scale reactor: Ferrate's efficacy in trifluralin degradation and products ecotoxicity evaluation. J Environ Chem Eng 12 (3), 112671. https://doi.org/10.1016/j.jece.2024.112671.
[25] Nguyen, T.B., Ho, P.N.T., Huang, C.P., Doong, R.-a, Chen, L., Chen, C.-W., Dong, C.-D., 2023. Peroxymonosulfate-assisted visible light sensitive 0D/3D Z-scheme NiCo2O4@g-C3N4 photocatalyst for effective degradation of ibuprofen in water. Chem Eng J 478. https://doi.org/10.1016/j.cej.2023.147332.
[26] Ni, B.-J., Yan, X., Dai, X., Liu, Z., Wei, W., Wu, S.-L., Xu, Q., Sun, J., 2020. Ferrate effectively removes antibiotic resistance genes from wastewater through combined effect of microbial DNA damage and coagulation. Water Res 185. https://doi.org/10.1016/j.watres.2020.116273.
[27] Pan, B., Feng, M., McDonald, T.J., Manoli, K., Wang, C., Huang, C.-H., Sharma, V. K., 2020. Enhanced ferrate(VI) oxidation of micropollutants in water by carbonaceous materials: elucidating surface functionality. Chem Eng J 398. https://doi.org/10.1016/j.cej.2020.125607.
[28] Pan, S., Yuan, D., Li, J., Wang, Z., Zhang, Q., Tang, S., 2024. Electron shuttle of carboxyl boosted Fe(III)-anchored carboxylated cellulose activating sodium perborate for organic pollutant abatement. Appl Catal B: Environ Energy 356, 124225. https://doi.org/10.1016/j.apcatb.2024.124225.
[29] Pawlus, K., Kwiatkowski, M., Stolarczyk, A., Glosz, K., Jarosz, T., 2022. Synthesis of explosive peroxides using unrecognised explosive precursors - percarbonates and perborates. FirePhysChem 2 (3), 285–293. https://doi.org/10.1016/j.fpc.2022.06.005.
[30] Peng, J., Zhou, P., Zhou, H., Liu, W., Zhang, H., Zhou, C., Lai, L., Ao, Z., Su, S., Lai, B., 2021. Insights into the electron-transfer mechanism of permanganate activation by graphite for enhanced oxidation of sulfamethoxazole. Environ Sci Technol 55 (13), 9189–9198. https://doi.org/10.1021/acs.est.1c00020.
[31] Peng, Y., Xie, G., Shao, P., Ren, W., Li, M., Hu, Y., Yang, L., Shi, H., Luo, X., 2022. A comparison of SMX degradation by persulfate activated with different nanocarbons: kinetics, transformation pathways, and toxicity. Appl Catal B-Environ Energy 310. https://doi.org/10.1016/j.apcatb.2022.121345.
[32] Piszcz-Karaś, K., Klein, M., Hupka, J., Łuczak, J., 2019. Utilization of shale cuttings in production of lightweight aggregates. J Environ Manag 231, 232–240. https://doi.org/10.1016/j.jenvman.2018.09.101.
[33] Ravindran, B., Mnkeni, P.N.S., 2016. Bio-optimization of the carbon-to-nitrogen ratio for efficient vermicomposting of chicken manure and waste paper using Eisenia fetida. Environ Sci Pollut Res 23 (17), 16965–16976. https://doi.org/10.1007/s11356-016-6873-0.
[34] Ren, W., He, Z., Shi, L., Xu, J., Li, C., Zhang, Y., Dong, K., Lee, S.-S., 2025. Mechanistic analysis and environmental impact assessment of ferrate degradation of sulfonamide antibiotics. Process Saf Environ Prot 194, 1257–1264. https://doi.org/10.1016/j.psep.2024.12.082.
[35] Roope, L.S.J., Smith, R.D., Pouwels, K.B., Buchanan, J., Abel, L., Eibich, P., Butler, C.C., Tan, P.S., Walker, A.S., Robotham, J.V., Wordsworth, S., 2019. The challenge of antimicrobial resistance: what economics can contribute, 41-+ Science 364 (6435). https://doi.org/10.1126/science.aau4679.
[36] Sabri, N.A., van Holst, S., Schmitt, H., van der Zaan, B.M., Gerritsen, H.W., Rijnaarts, H.H.M., Langenhoff, A.A.M., 2020. Fate of antibiotics and antibiotic resistance genes during conventional and additional treatment technologies in wastewater treatment plants. Sci Total Environ 741. https://doi.org/10.1016/j.scitotenv.2020.140199.
[37] Sharma, V.K., 2013. Ferrate(VI) and ferrate(V) oxidation of organic compounds: Kinetics and mechanism. Coord Chem Rev 257 (2), 495–510. https://doi.org/10.1016/j.ccr.2012.04.014.
[38] Sharma, V.K., Mishra, S.K., 2006. Ferrate(VI) oxidation of ibuprofen: a kinetic study. Environ Chem Lett 3 (4), 182–185. https://doi.org/10.1007/s10311-005-0002-5.
[39] Sun, S., Jiang, J., Qiu, L., Pang, S., Li, J., Liu, C., Wang, L., Xue, M., Ma, J., 2019. Activation of ferrate by carbon nanotube for enhanced degradation of bromophenols: kinetics, products, and involvement of Fe(V)/Fe(IV). Water Res 156, 1–8. https://doi.org/10.1016/j.watres.2019.02.057.
[40] Sun, Y., Zhao, L., Teng, Y., 2020. Effect of soil type on the degradation of polychlorinated biphenyls in a pyrophosphate-chelated Fenton-like reaction. Chem Eng J 390, 124574. https://doi.org/10.1016/j.cej.2020.124574.
[41] Wang, P., Wen, L., Dong, C., Lin, L., Yang, C., Li, X.-y, 2024. Iron–molybdenum bimetals incorporated montmorillonite-based catalytic ceramic membrane for heterogenous Fenton reaction towards the degradation of micropollutants in water. Chem Eng J 500, 156833. https://doi.org/10.1016/j.cej.2024.156833.
[42] Wang, Q., Zhang, Y., Yang, Y., Fu, H., Liang, Y., Ma, J., 2023. Zero valent copper-mediated ferrate (VI) for the degradation of bisphenol AF. J Environ Chem Eng 11 (3), 109600. https://doi.org/10.1016/j.jece.2023.109600.
[43] Wang, Z., Yang, X., Du, Q., Liu, T., Dai, X., Du, Y., Zhang, H., Zhou, P., Xiong, Z., Lai, B., 2024. Ferrate(VI)/percarbonate for the oxidation of micropollutants: Interactive activation and release of low-concentration hydrogen peroxide for efficient electron utilization. J Hazard Mater 469, 134029. https://doi.org/10.1016/j.jhazmat.2024.134029.
[44] Widhiastuti, F., Fan, L., Paz-Ferreiro, J., Chiang, K., 2021. Oxidative treatment of bisphenol A in municipal wastewater reverse osmosis concentrate using Ferrate (VI). J Environ Chem Eng 9 (4), 105462. https://doi.org/10.1016/j.jece.2021.105462.
[45] Wu, S., Shen, L., Lin, Y., Yin, K., Yang, C., 2021. Sulfite-based advanced oxidation and reduction processes for water treatment. Chem Eng J 414, 128872. https://doi.org/10.1016/j.cej.2021.128872.
[46] Xu, J., Li, C., He, Z., Chen, Z., Zhang, K., Ren, W., Zhang, Y., Guan, X., 2025. A green method on dipole solvent as "Activators": γ-valerolactone/H2O system promoted degradation of ciprofloxacin by ferrate(VI). Water Res 271, 122991. https://doi.org/10.1016/j.watres.2024.122991.
[47] Yang, Y., Li, X., Yin, H., Xu, X., Guan, Q., Chen, C., 2025. Enhancing degradation of micropollutants and utilization of ferrate by oxygen-vacancy-activated ferrate species on CeO2. Chem Eng J 504, 159021. https://doi.org/10.1016/j.cej.2024.159021.
[48] Yao, B., Lu, Y., Li, A., Ma, L., Wang, W., Wu, K., Ji, Y., Zhu, F., Chen, J., Lu, J., 2024. Ferrate(VI) oxidative degradation of capecitabine in aquatic matrices: degradation performance, mechanisms, and toxicity assessment. J Environ Chem Eng 12 (6), 114535. https://doi.org/10.1016/j.jece.2024.114535.
[49] Yue, X., Shan, Y., Jiao, W., Shen, K., Zhang, Y., 2023. Role of direct current on thermal activated peroxydisulfate to degrade phenanthrene in soil: conversion of sulfate radical and hydroxyl radical to singlet oxygen, accelerated degradation rate and reduced efficiency. J Hazard Mater 452, 131187. https://doi.org/10.1016/j.jhazmat.2023.131187.
[50] Zhang, H., Deng, S., Zhu, L., Liu, Y., 2024. Degradation of sulfamethoxazole in a falling film dielectric barrier discharge system: performance, mechanism and toxicity evaluation. Sci Total Environ 956, 177320. https://doi.org/10.1016/j.scitotenv.2024.177320.
[51] Zhang, H., Luo, M., Zhou, P., Liu, Y., Du, Y., He, C., Yao, G., Lai, B., 2022. Enhanced ferrate(VI)) oxidation of sulfamethoxazole in water by CaO2: the role of Fe(IV) and Fe(V). J Hazard Mater 425. https://doi.org/10.1016/j.jhazmat.2021.128045.
[52] Zhao, J., Wang, Q., Fu, Y., Peng, B., Zhou, G., 2018. Kinetics and mechanism of diclofenac removal using ferrate(VI): roles of Fe3+ , Fe2+ , and Mn2+. Environ Sci Pollut Res 25 (23), 22998–23008. https://doi.org/10.1007/s11356-018-2375-6.
[53] Zhao, X.-N., Huang, Z.-S., Liu, Y.-L., Gu, H.-T., Gao, Z., Cui, C., Ma, J., Wang, L., 2025. Roles of iron (V) and iron (IV) species in ferrate-triggered oxidation of phenolic pollutants and their transformation induced by phenoxyl radical. Water Res 274, 123133. https://doi.org/10.1016/j.watres.2025.123133.
[54] Zhou, J., Tian, Y., Yan, C., Li, D., Liu, T., Liu, G., Chen, D., Feng, Y., 2024. Potassium peroxoborate: a sustained-released reactive oxygen carrier with enhanced PAHs contaminated soil remediation performance. J Hazard Mater 470, 134259. https://doi.org/10.1016/j.jhazmat.2024.134259.
[55] Zhou, J., Tian, Y., Yan, C., Li, D., Liu, T., Liu, G., Chen, D., Feng, Y., 2024. Potassium peroxoborate: a sustained-released reactive oxygen carrier with enhanced PAHs contaminated soil remediation performance. J Hazard Mater 470. https://doi.org/10.1016/j.jhazmat.2024.134259.
[56] Zhu, J., Yu, F., Meng, J., Shao, B., Dong, H., Chu, W., Cao, T., Wei, G., Wang, H., Guan, X., 2020. Overlooked role of Fe(IV) and Fe(V) in organic contaminant oxidation by Fe(VI). Environ Sci Technol 54 (15), 9702–9710. https://doi.org/10.1021/acs.est.0c03212.